

The chemical composition of the Herbig Ae SB2 system AK Sco (HD 152404)

F. Castelli^{1†}, S. Hubrig^{2‡}, S. P. Järvinen², M. Schöller³

¹*Istituto Nazionale di Astrofisica – Osservatorio Astronomico di Trieste, Via Tiepolo 11, 34131 Trieste, Italy*

²*Leibniz-Institut für Astrophysik Potsdam (AIP), An der Sternwarte 16, 14482 Potsdam, Germany*

³*European Southern Observatory, Karl-Schwarzschild-Str. 2, 85748 Garching, Germany*

Accepted XXX. Received YYY; in original form ZZZ

ABSTRACT

We investigate the stellar atmospheres of the two components of the Herbig Ae SB2 system AK Sco to determine the elements present in the stars and their abundance. Equal stellar parameters $T_{\text{eff}} = 6500$ K and $\log g = 4.5$ were used for both stars. We studied HARPSpol spectra (resolution 110 000) that were previously used to state the presence of a weak magnetic field in the secondary. A composite synthetic spectrum was compared in the whole observed region $\lambda\lambda$ 3900–6912 Å with the observed spectrum. The abundances were derived mostly from unblended profiles, in spite of their sparsity, owing to the complexity of the system and to the not negligible $v \sin i$ of 18 km s^{-1} and 21 km s^{-1} adopted for the two components, respectively. The identified elements are those typical of stars with spectral type F 5 IV–V, except for Li I at 6707 Å and He I at 5875.61 Å, whose presence is related with the Herbig nature of the two stars. Furthermore, overabundances were determined in both stars for Y, Ba, and La. Zirconium is overabundant only in the primary, while sulfur is overabundant outside the adopted error limits only in the secondary. In contrast to previous results showing a high occurrence rate of λ Boo peculiarities or normal chemical composition among the Herbig Ae/Be stars, the abundance pattern of AK Sco is similar to that of only few other Herbig stars displaying weak Ap/Bp peculiarities. A few accretion diagnostic lines are discussed.

Key words: line: identification – atomic data – stars: atmospheres – stars: chemically peculiar – stars: individual: AK Sco

1 INTRODUCTION

The combination of knowledge about the magnetic field structure and the determination of the stellar chemical composition is very likely the key to constrain theories on star formation and magnetospheric accretion in intermediate-mass Herbig Ae/Be stars. These stars are surrounded by active accretion disks and most of the excess emission present at various wavelengths can probably be ascribed to the interaction of the disk with a magnetically active star (e.g. Muzerolle et al. 2004).

Magnetic Herbig Ae/Be stars are frequently considered as precursors of the magnetic Ap stars (e.g. Stepień & Landstreet 2002; Catala 2003). However, in contrast to chemical peculiar magnetic Ap stars, for which the abundance anomalies are believed to be produced by mechanisms intrinsic to the stars themselves, such as radiatively

driven diffusion (e.g. Michaud 1970), the photospheric material in Herbig Ae/Be stars is mixed with circumstellar material originating in a protoplanetary disk. Therefore, studies of photospheric composition in these stars can also provide information on protoplanetary material.

Only very few abundance analyses of Herbig Ae/Be stars were carried out in the past. Cowley et al. (2010) reported on a chemical composition similar to that in λ Boo stars in the magnetic Herbig Ae star HD 101412. Later-on, Folsom et al. (2012) reported on the abundance analysis of 20 Herbig Ae/Be stars, concluding that half the stars in their sample show λ Boo chemical peculiarities. Only one star in their study showed weak Ap/Bp peculiarities and all the remaining stars were chemically normal. In contrast, the abundance study of the double-lined spectroscopic binary (SB2) system HD 104237 by Cowley, Castelli & Hubrig (2013) showed slight enhancements of a few elements, where the case for Zr was the strongest. The Herbig Ae star PDS 2 was studied by Cowley, Hubrig & Przybilla (2014) and found to have λ Boo characteristics.

† Deceased.

‡ Corresponding author: shubrig@aip.de

AK Sco (HD 152404) is a double-lined spectroscopic binary system formed by two nearly identical Herbig Ae stars (F5 V spectral type) surrounded by a circumbinary disk. Furthermore, the gap between the stars and the disk is filled by some gas. The Herbig nature of AK Sco was first stated by [Herbig & Kameswara Rao \(1972\)](#), who observed H α emission with a deep reversal and Li I absorption at 6707 Å in Coudé spectrograms. However, according to [Andersen et al. \(1989\)](#), a follow-up observation with the ESO 1.5 m telescope on La Silla in 1986 did not reveal the presence of emission lines in the blue spectral region. On the other hand, this observation showed doubling of all photospheric spectroscopic lines, indicating that AK Sco is a spectroscopic binary with approximately equal components. Subsequent radial-velocity observations discovered that it is indeed a SB2 system with a short period (13.6 days) and large eccentricity ($e = 0.47$) ([Andersen et al. 1989](#)).

[Alencar et al. \(2003\)](#) reconsidered the orbital parameters and the physical elements of the system finding a substantial agreement with the results of [Andersen et al. \(1989\)](#). Furthermore, [Alencar et al. \(2003\)](#) inferred the pre-main-sequence (PMS) nature of the secondary from the presence of the strong Li I line at 6707 Å in the spectrum. A characteristic of AK Sco is the light variability, which was shown to be related to a variable circumstellar obscuration ([Andersen et al. 1989](#); [Alencar et al. 2003](#)) rather than to the orbital motion of the two components. Recent spectropolarimetric observations using HARPSpol spectra, performed at six different orbital phases ($\phi = 0.946, 0.950, 0.018, 0.025, 0.090$, and 0.169), indicated the presence of a weak magnetic field of the order of 80 G in the secondary component at the phase 0.090 ([Järvinen et al. 2018](#)). This discovery raised the question whether chemical peculiarities like those observed in the main sequence Ap stars can be observed also in AK Sco.

There are only few studies on the chemical composition of magnetic Herbig Ae/Be stars. [Folsom et al. \(2012\)](#) analyzed the abundances in a sample of 21 Herbig Ae/Be stars. Three of them are affected by the presence of a magnetic field. They found that the magnetic Herbig stars do not exhibit a chemical composition remarkably different from the normal stars. One of them (HD 101412) displays λ Boo chemical peculiarities, another (V 380 Ori A) shows weak Ap/Bp peculiarities, and the third one (HD 190073) was found to be normal. The chemical composition of HD 101412 and HD 190073 was also studied by [Cowley et al. \(2010\)](#) and [Cowley & Hubrig \(2012\)](#), respectively. Their results roughly agree with those from [Folsom et al. \(2012\)](#). In addition, [Cowley, Castelli & Hubrig \(2013\)](#) and [Cowley, Hubrig & Przybilla \(2014\)](#) analyzed the spectra of two other magnetic Herbig Ae stars, HD 104237 and PDS2. The presence of a magnetic field was dubious for PDS2, until [Hubrig et al. \(2015\)](#) definitively detected it.

Abundances for fourteen magnetic (including HD 104237) and non-magnetic Herbig Ae/Be stars were also presented by [Acke & Waelkens \(2004\)](#). Both [Cowley, Castelli & Hubrig \(2013\)](#) and [Acke & Waelkens \(2004\)](#) demonstrated that the abundances of HD 104237 are slightly peculiar with enhanced elements Y, Zr, Ba, and La. The agreement between the results from the two studies concerning these elements is within 0.07 dex. In contrast,

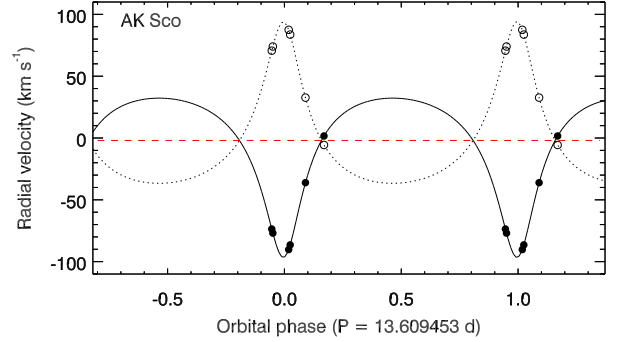


Figure 1. Radial velocity curve from the orbital solution from [Alencar et al. \(2003\)](#). The circles indicate the phases of our observations. Star A (black filled circles) has its minimum velocity at phase 0.00.

the chemical composition of PDS2 was found to be similar to that of the λ Boo stars.

In this paper we use HARPSpol spectra covering the 3900–6912 Å region to investigate the composite spectrum of AK Sco with the aim to increase the number of abundance analyses of magnetic Herbig Ae/Be stars.

2 OBSERVATIONS

We used the same HARPSpol spectropolarimetric observations of AK Sco and the same reduced spectra that are described in [Järvinen et al. \(2018\)](#). Here we recall that the observations cover six orbital phases (0.946, 0.950, 0.018, 0.025, 0.090, 0.169) of the binary system. The covered orbital phases (calculated using the orbital solution from [Alencar et al. \(2003\)](#)) are presented in Fig. 1. While the observed wavelength interval is 3780–6912 Å, with a small gap between 5259 and 5337 Å, the region useful for the analysis starts at 3900 Å because the noise is too strong at lower wavelengths. The resolving power is about 110 000.

In this work, the normalization to the continuum performed by [Järvinen et al. \(2018\)](#) was adjusted at intervals of 6 Å by comparing observed and computed spectra. The continuum level was lowered from about 30% at 4000 Å, to about 5% at 4600 Å, to 0.05–0.25% for $\lambda > 5000$ Å. In all the spectra, except for that at the phase 0.169, the spectral lines of both components are well separated. The variability was studied by using all six spectra observed at the different epochs.

3 STELLAR PARAMETERS AND SYNTHETIC SPECTRA

The abundances were derived from the spectrum observed at the phase $\phi = 0.090$, i.e. from the spectrum for which the presence of a weak magnetic field was established ([Järvinen et al. 2018](#)). Furthermore, at this phase the two stars are well separated with a radial velocity shift $\Delta v = 74 \text{ km s}^{-1}$ (see Table 1).

The double-line spectrum, the similar intensity of the lines from the two stars, and the rather high rotational velocities (18 km s^{-1} and 21 km s^{-1} , respectively) increase the number of blended profiles, so that it is very difficult to pick

Table 1. Observed phases, difference in radial velocity between the two components, the radial velocity of the primary, and the luminosity fraction (in %) observed from the secondary.

	Date	Phase	$v_r(B)-v_r(A)$ [km s ⁻¹]	$v_r(A)$ [km s ⁻¹]	$\frac{L(B_{\text{obs}})}{L(B_{\text{tot}})}$ [%]
1	2016-06-15	0.946	138	-70	10
2	2017-06-04	0.950	146	-72.5	50
3	2016-06-18	0.018	180	-90	50
4	2017-06-05	0.025	177	-87	80
5	2017-06-06	0.090	74	-36	100
6	2017-06-07	0.169	1.	0.	100

up lines that do not have any contamination with lines either from the same star or from the companion. Therefore, the whole analysis was performed with the synthetic spectrum method. Unblended lines are rare, so that the abundance for a given element was determined from the profiles of few single lines, when available. Then the abundance was checked on blended lines having the element as main or sometimes even minor component of the blend.

The atomic and molecular line lists adopted to compute the synthetic spectra were produced by Castelli¹, who assembled the line lists from the GFNEW directory (Kurucz 2018), available at the Kurucz website², with line lists taken from the literature for some ions missing in the Kurucz data. Furthermore, if needed, the $\log g$ values in the Kurucz line lists were replaced by values either extracted from various literature sources or obtained by fitting the solar synthetic spectrum to the observed solar flux Atlas from Kurucz (2005a). For numerous lines, Van der Waals broadening was computed according to the Anstee & O'Mara (1995) theory. The γ_{vdw} and α parameters were taken from the Barklem, Piskunov & O'Mara (2000) tables.

We adopted for both stars $T_{\text{eff}} = 6500$ K from Andersen et al. (1989), who inferred this temperature on the basis of the F5 V spectral type. They used the T_{eff} – spectral type calibration given by Bessell (1979) and by Popper (1980). For this value of T_{eff} , Alencar et al. (2003) determined the system parameters assuming nearly identical components, in particular $M = 1.35 \pm 0.07 M_{\odot}$, $R = 1.59 \pm 0.35 R_{\odot}$, and $v \sin i = 18.5 \pm 1 \text{ km s}^{-1}$, provided that the stellar inclination is between 65 and 70 degrees. The gravity, deduced from the mass and radius given above, is $\log g = 4.16 \pm 0.25$.

In order to check the gravity obtained from mass and radius spectroscopically, we used the wings of the Mg I triplet at 5167.321, 5172.684, and especially 5183.604 Å, because it does not show the slight redshift as the other two lines do. At first, we determined the Mg abundance $\log(N_{\text{Mg}}/N_{\text{tot}}) = -4.55$ for $T_{\text{eff}} = 6500$ K and $\log g = 4.16$ using the Mg II line at 4481 Å, which is almost independent of gravity. For this abundance and $\log g = 4.16$ the computed wings of the Mg I triplet were too narrow. To improve the agreement between the observed and computed Mg I profiles we increased the gravity to $\log g = 4.5$ (Fig. 2). We note that when the line data were checked on the solar spectrum, we

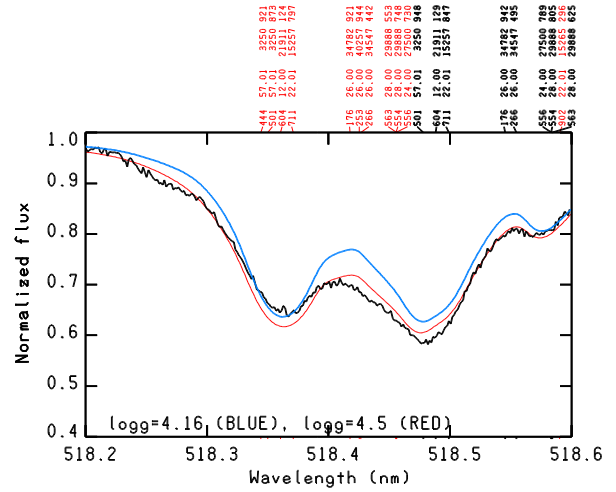


Figure 2. Comparison of the Mg I profile at 5183.604 Å observed in the composite spectrum at the phase 0.090 (black line) with two spectra computed with solar magnesium abundance, the same $T_{\text{eff}} = 6500$ K, and two different $\log g = 4.16$ (blue line) and 4.5 (red line). The red and black labels identify the lines observed in the primary and in the secondary, respectively. The wavelength scale corresponds to the laboratory wavelengths of the primary. The identification labels of the secondary have to be read on wavelength scale corresponding to the laboratory wavelengths of the secondary (i.e. 5184.604 for the secondary has to be read 5183.604).

decreased for the Mg I triplet the parameter $\log \gamma_{\text{vdw}}$ from -7.27 , as given by Barklem, Piskunov & O'Mara (2000), to -7.37 . Probably, a different solar model than that used by us would have given good agreement between observed and computed wings of the solar Mg I triplet for $\log \gamma_{\text{vdw}} = -7.27$. For the Sun, we adopted an ATLAS9 model with parameters $T_{\text{eff}} = 5777$ K and $\log g = 4.4377$, and turbulent velocity $\xi = 1 \text{ km s}^{-1}$. This model was used because it is consistent with the ATLAS9 model adopted to analyze AK Sco.

An ATLAS9 model atmosphere with parameters $T_{\text{eff}} = 6500$ K and $\log g = 4.5$ from the updated Castelli & Kurucz (2004)³ grid was used to compute synthetic spectra for both components by means of the SYNTH code (Kurucz 2005b). On the basis of the comparison of the observed and computed profiles, the microturbulent velocity was estimated to be $\xi = 1 \text{ km s}^{-1}$ and $\xi = 2 \text{ km s}^{-1}$ for the primary and the secondary, respectively. The rotational velocity $v \sin i$ was determined from the comparison of observed and computed profiles of numerous stellar features (e.g. Mg II 4481 Å). We adopted the values 18 km s^{-1} and 21 km s^{-1} for the primary and the secondary, respectively. Finally, the computed profiles were broadened for a Gaussian instrumental profile, corresponding to the resolving power 110 000 of the HARPSpol spectrum.

The composite spectrum was obtained with the BINARY code (Kurucz 1995). As described by Cowley, Castelli & Hubrig (2013), the spectra of the two components are shifted in respect to each other in accordance with the observed radial velocity difference. Then, they were weighted with the luminosity ratio and added

¹ <http://wwwuser.oats.inaf.it/castelli/linelists.html>

² <http://kurucz.harvard.edu/linelists.html>

³ <http://wwwuser.oats.inaf.it/castelli/grids.html>

together. The adopted luminosity ratio is 1.0, corresponding to a radii ratio equal to 1.0 (Gómez de Castro 2009). Because not only all the accretion diagnostic lines, but also photospheric lines show intensity variations over the observing nights (Järvinen et al. 2018), we investigated whether the photospheric line variability may be caused by abundance changes. By comparing observed and computed spectra at different phases, we concluded that the variability of the photospheric lines should be mostly related to the presence of the circumbinary disk, which obscures the secondary component with dust clouds with different densities at different phases. We assumed “a priori” that there is no obscuration at the phase 0.090, so that we adopted as stellar abundances those derived at this phase. For the other phases, we determined for the secondary the fraction in percent of the observed luminosity to its total luminosity on the basis of the Li I profile at 6707 Å. We assumed that the abundance of Li I in all phases is the same as that at the phase 0.090. Table 1 summarizes for the different phases the radial velocity difference for the two stars, the radial velocity of the primary as determined from the spectra, and the observed luminosity fraction (in %) of the secondary.

4 IDENTIFICATION AND ABUNDANCES

The whole available spectrum from 3900 Å to 6900 Å was synthesized and compared with the HARPSpol spectrum. In order to derive the abundances, we analyzed the profiles of the lines listed in the Appendix. The comparison of the observed spectrum with the spectrum computed with the final abundances listed in Table 2 is available from Castelli’s webpage⁴. We identified in both stars: H I, Li I, C I, O I, Na I, Mg I, Mg II, Al I, Si I, Si II, S I, Ca I, Ca II, Sc I, Sc II, Ti I, Ti II, V I, V II, Cr I, Cr II, Mn I, Fe I, Fe II, Co I, Ni I, Cu I, Zn I, Sr I, Sr II, Y II, Zr II, Ba I, Ba II, La II, Ce II, and Nd II. In addition, He I at 5876.61 Å is observed according to the Herbig nature of the studied stars. We note that for a temperature of 6500 K, He I is not predicted, unless it is unreasonably overabundant. Predicted marginal contributions from CH and CN are not in conflict with the observations.

Most lines for all elements are well reproduced in the observed spectra by solar abundances for both components, except for Li, Sr, Y, Ba, and La. Zirconium is overabundant only in the primary. Sulfur is overabundant by 0.3 dex in the secondary, while we considered its overabundance of 0.2 dex in the primary as solar abundance within the error limits (see Table 2). The adopted solar abundance for neodymium is a lower limit, because we can not exclude some overabundance also for this element. While some lines are well fitted by solar abundances, some others are computed too weak. These discordant results can be related to the weakness and the blending of the Nd II lines as well as with the adopted $\log gf$ values. The solar abundances listed in Col. 6 of Table 2 are from Asplund et al. (2009), Scott et al. (2015a), Scott et al. (2015b), and Grevesse et al. (2015).

Some lines are affected by a variable additional absorption that has become recognizable due to a slightly redshifted wavelength or a too broad profile as compared with the computed one. In some cases, the observed core is flatter than that predicted by the synthetic spectrum. Abundances from these lines may differ from those derived from other lines of the same element.

The comparison between the observed spectra at all phases with the computed spectrum indicates that for all elements most lines are well fitted by the same adopted abundances. Therefore, the variability observed and discussed in previous works has to be ascribed to the relative position of the two components, to the circumbinary disk, to the presence of some gas between the disk and the components, rather than to abundance spots over the stellar surfaces.

The main uncertainty sources in the abundance determination are the location of the continuum level, the $\log gf$ values, and missing lines in the line lists. For weak and medium-strong lines a change in the continuum level by 10% results in an uncertainty of about 0.1 dex for the abundance. We assumed a total error of ± 0.20 dex as the maximum error for the adopted abundances.

5 LINE PROFILES NOT WELL REPRODUCED BY THE LTE SYNTHETIC SPECTRUM

While large parts of the spectrum are well reproduced by the LTE synthetic spectrum using the abundances listed in Table 2, there are some profiles which require more sophisticated models and methods to be explained in a satisfactory way. They are mostly features affected by magnetospheric activity, such as the Balmer profiles, He I 5875.61 Å, and the Na I D lines, which were also discussed by Pogodin et al. (2012). In addition, also the Ca II K and H lines, the strongest lines of Mg I, and some lines of Fe I show signatures of stellar activity. The list of the not well reproduced line profiles is given below.

Balmer lines: Only H α shows emission. It is present in all six phases. The profiles differ each from the other for both the emission and absorption contributions, and differ also from the profiles displayed by Alencar et al. (2003), which were observed at phases (i.e. $\phi = 0.05, 0.17, 0.57$, and 0.81) different from those we studied in this paper. The H β profiles are in absorption in all observed phases, although they display a strong variability. They are formed by a strong deep absorption core, not predicted by the model, and by an additional absorption, redshifted by a few Angstrom, which is observable in all phases, except for the phase at 0.169, where the observed and computed central wavelengths coincide. As a consequence, except for the phase at 0.169, the whole observed H β profile is redshifted and broader than that predicted by the model. The H β profiles discussed here are similar to those shown by Alencar et al. (2003). The same behaviour can be observed also in the H γ and H δ profiles, although to a lesser extent than that observed for H β .

He I: The line of He I at 5875.61 Å is well observable in both components as a weak variable absorption (Fig. 3). It can not be predicted by the synthetic spectrum, whichever helium abundance is adopted. No other He I lines are present in the HARPSpol spectrum. Reiter et al. (2018) studied He I $\lambda 10830$ line profiles in a sample of Herbig Ae/Be stars and

⁴ http://wwwuser.oats.inaf.it/castelli/stars/AK_Sco/AK_Sco.html

Table 2. Abundances $\log(N_{\text{elem}}/N_{\text{tot}})$ of the identified elements in AK Sco. Solar abundances are from [Asplund et al. \(2009\)](#), [Scott et al. \(2015a,b\)](#), and [Grevesse et al. \(2015\)](#). The values in round brackets in Cols. 2 and 4 denote the numbers of lines used in the spectral analysis of that ion. The values in square brackets in Cols. 3 and 5 denote the differences between the abundance found in AK Sco and the solar abundance.

Element	A component ($T_{\text{eff}} = 6500 \text{ K}$, $\log g = 4.5$)		B component ($T_{\text{eff}} = 6500 \text{ K}$, $\log g = 4.5$)		Sun
Li I	-8.70 (1)	[+2.29]	-8.50 (1)	[+2.49]	-10.99
C I	-3.61 (1)	[0.00]	-3.61 (1)	[0.00]	-3.61
O I	-3.35 (3)	[0.00]	-3.35 (3)	[0.00]	-3.35
Na I	-5.93 (2)	[-0.10]	-5.78±0.05 (3)	[+0.05]	-5.83
Mg I	-4.55 (2)	[-0.10]	-4.45 (3)	[+0.00]	-4.45
Mg II	-4.55 (1)	[-0.10]	-4.45 (1)	[+0.00]	-4.45
Al I	-5.61 (2)	[0.00]	-5.61 (2)	[+0.00]	-5.61
Si I	-4.40±0.07 (12)	[+0.13]	-4.31±0.06 (7)	[+0.22]	-4.53
Si II	-4.40 (1)	[+0.13]	-4.40 (1)	[+0.13]	-4.53
Si _{tot}	-4.40±0.07	[+0.13]	-4.33±0.07	[+0.20]	-4.53
S I	-4.72±0.10 (2)	[+0.20]	-4.62±0.10 (2)	[+0.30]	-4.92
Ca I	-5.70±0.10 (15)	[+0.02]	-5.84±0.08 (12)	[-0.12]	-5.72
Sc II	-8.98 (3)	[-0.10]	-8.68 (2)	[+0.20]	-8.88
Ti I	-7.14±0.04 (3)	[-0.03]			-7.11
Ti II	-6.88±0.09 (6)	[+0.23]	-7.14±0.09 (3)	[-0.03]	-7.11
Ti _{tot}	-6.96±0.15	[+0.15]	-7.14±0.09	[-0.03]	-7.11
V I	-8.15 (2)	[0.00]			-8.15
Cr I	-6.41±0.12 (4)	[+0.01]	-6.42 (3)	[0.00]	-6.42
Cr II	-6.22±0.20 (2)	[+0.20]	-6.35±0.04 (3)	[+0.07]	-6.42
Cr _{tot}	-6.34±0.17	[+0.08]	-6.39±0.02	[+0.03]	-6.42
Mn I	-6.62 (3)	[0.00]	-6.62 (2)	[0.00]	-6.62
Fe I	-4.66±0.15 (12)	[-0.11]	-4.51±0.17 (11)	[+0.06]	-4.57
Fe II	-4.42 (2)	[+0.15]	-4.44±0.06 (5)	[+0.13]	-4.57
Fe _{tot}	-4.62±0.16	[-0.05]	-4.49±0.15	[+0.08]	-4.57
Co I			-6.91 (1)	[+0.20]	-7.11
Ni I	-5.84±0.08 (9)	[0.00]	-5.74±0.17 (8)	[+0.14]	-5.84
Cu I	-7.86 (1)	[0.00]	-7.86 (1)	[+0.00]	-7.86
Zn I	-7.38 (2)	[+0.10]	-7.58 (2)	[-0.10]	-7.48
Sr I			-9.00 (1)	[+0.21]	-9.21
Sr II	-9.10 (1)	[+0.11]	-8.90 (1)	[+0.29]	-9.21
Sr _{tot}	-9.10	[+0.11]	-8.95±0.05	[+0.24]	-9.21
Y II	-9.40 (2)	[+0.40]	-9.50 (1)	[+0.30]	-9.83
Zr II	-9.05 (2)	[+0.40]	-9.45 (1)	[0.00]	-9.45
Ba II	-9.51 (1)	[+0.28]	-9.41 (1)	[+0.38]	-9.79
La II	-10.22±0.15 (2)	[+0.71]	-10.57 (1)	[+0.36]	-10.93
Ce II	-10.46 (1)	[+0.00]			-10.46
Nd II	-10.62 (1)	[+0.00]	-10.62	[+0.00]	-10.62

reported that in the near-IR spectrum of AK Sco this line appears partially in emission.

Na I: The Na I doublet displays a composite structure. In the primary (Fig. 4), the line observed at 5889.950 Å is well predicted at the phases 0.946, 0.950, 0.018, and 0.025, while it is stronger than the computed one at the phases 0.090 and 0.169. The other line at 5895.920 Å is well predicted at the phases 0.946 and 0.950, but it is computed too weak for all the other phases. In the secondary (Fig. 5), the Na I doublet is well reproduced only at the phase 0.946, while in all other phases the observed line is stronger than the computed one, especially at the phases 0.090 and 0.169. The profiles are affected by a blue-shifted strong broad component, probably due to the magnetospheric interaction with the accretion disk. Narrow interstellar Na I lines are also present in the spectrum in all the observed phases.

Mg I: In the primary, the line core is weaker than the computed one in almost all observed lines ($\lambda\lambda$ 4702.091,

5167.321, 5172.684, 5183.604, and 5228.405 Å). Furthermore, the lines at 5167.321 and 5172.684 Å are redshifted by 1.5 km s^{-1} , corresponding to $\Delta\lambda = 0.025 \text{ Å}$. In the secondary, the Mg I profiles are well reproduced both in shape and position.

Al I: The resonance line at 3944.006 Å is redshifted by 3 km s^{-1} , corresponding to $\Delta\lambda = 0.04 \text{ Å}$.

Si I: The Si I line at 6237.319 Å is variable. It is computed too strong in all phases.

Ca I: Only in the secondary, a few lines of Ca I are stronger than the predicted ones. Among them, the line at 4226.728 Å is blended, those at 5590.114 and 6122.217 Å display an observed core stronger than the computed one, while the line at 6717.081 Å is either blended with an unknown component, or is affected by an additional redshifted absorption. This line is unshifted at the phase 0.090 and redshifted at the other phases.

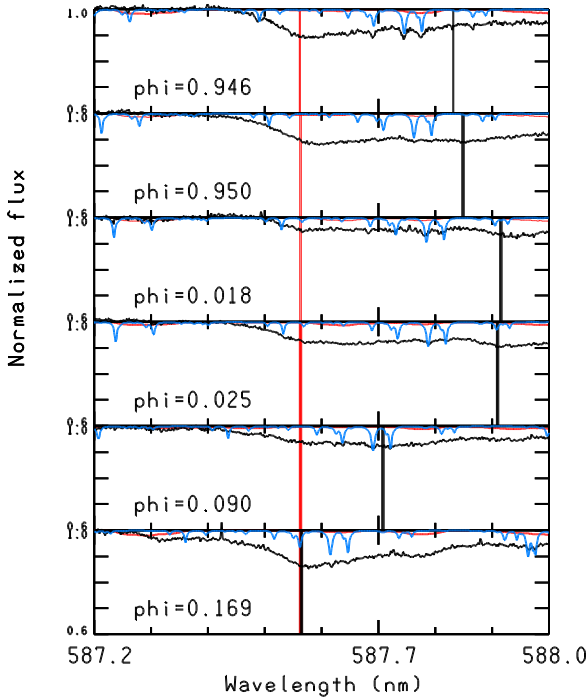


Figure 3. The He I line at 5875.6 Å arising in the magnetospheric accretion flow observed at six different phases in AK Sco. The red and black vertical lines mark the position of He I in the primary and in the secondary, respectively. The sharp blue lines indicate contamination by telluric lines.

Ca II: For both Ca II K and H profiles the core is flat and weaker than the computed one with a different shape at different phases (Fig. 6).

Fe I: Several Fe I lines display an observed core weaker than the computed one. Examples are the strong lines of Fe I at 4920.502, 4957.596, 4991.268, 5007.274, 5110.413, 5367.465, 5424.067, and 5445.042 Å. Other Fe I lines seem to be double, or both double and redshifted. For instance, for the primary, the observed core of the Fe I profiles at 5615.644 Å is weaker than the computed one and is redshifted by 0.01 Å at the phase 0.025.

Fe II: The line at 5018.436 Å is redshifted by about 0.05 Å at the phase 0.025, but it is centered at the laboratory wavelength at the other phases. However, the observed profile is always stronger and broader than the predicted one.

6 DISCUSSION

Among the Herbig Ae stars, close spectroscopic binaries with orbital periods below 20 days are very rare (Duchêne 2015). This might be the result of merger events early at the pre-main-sequence stage, in line with recent observations of magnetic Ap and Bp stars, suggested to be successors of the magnetic Herbig Ae/Be stars on the main-sequence. According to Ferrario et al. (2009), at least one of the merging stars must be on the Heney part of the pre-main-sequence track towards the end of its contraction to the main sequence. The merger outcome then becomes observable as a magnetic Herbig Ae/Be star. This implies that there should be almost no

magnetic star in close Herbig Ae/Be and Ap/Bp binaries. Indeed, previous studies of main-sequence binary systems with A- and late B-type primaries detected only two systems, HD 98088 and HD 161701, with a magnetic Ap star as a component (Babcock 1958; Hubrig et al. 2014). Therefore, the combination of the determination of the chemical composition and studies of the magnetic field structure in close binary components plays an important role for understanding the mechanisms that can be responsible for the generation of magnetic fields.

Figure 7 shows that the abundance patterns of the first (red crosses) and second (red boxes) components of AK Sco have the same trend, although they are not identical. In both stars, most of the elements have solar or nearly solar abundances. In addition to Li (not included in Fig. 7), exceptions are found for Si, S, Y, Zr, Ba, and La, which are overabundant. The overabundance in the primary and in the secondary are correspondingly [2.3] and [2.5] for Li, [0.13] and [0.20] for Si, [0.20] and [0.30] for S, [0.4] and [0.3] for Y, [0.28] and [0.38] for Ba, [0.71] and [0.36] for La. Zirconium is overabundant by [0.4] only in the primary, while it was found solar in the secondary. In addition to this large abundance difference for Zr II, other remarkable differences are those for Sc II (0.30 dex), Ti II (0.29 dex), and La II (0.35 dex). Because we estimate that the errors in the abundance determination are at least of the order of 0.2 dex, we prefer to consider the abundance differences from the two components lower than 0.2 dex as not conclusive.

In Fig. 7 we compare the abundances of the two components of AK Sco with the abundances of the two magnetic Herbig Ae stars HD 104237 (Cowley, Castelli & Hubrig 2013) and PDS2 (Cowley, Hubrig & Przybilla 2014). While the abundance patterns of both components in the studied SB2 system, AK Sco A and AK Sco B, are similar to the abundance pattern of the primary in the SB2 system HD 104237 (open circles), in particular for elements heavier than strontium, they are rather different from the abundance pattern of the single Herbig star PDS2 (triangles), which follows the trend shown by the λ Boo stars.

In conclusion, although AK Sco B, HD 104237, and PDS2 are magnetic stars, they do not have a similar abundance behaviour: the first two stars display weak Ap/Bp peculiarities, as well as AK Sco A does, although no magnetic field was detected up to now for it. In contrast, PDS2 is characterized by λ Boo chemical peculiarities. The two different kinds of abundance patterns (Ap/Bp and λ Boo) do not seem to be dependent on temperature, since PDS2 and AK Sco have the same $T_{\text{eff}} = 6500$ K.

ACKNOWLEDGEMENTS

Based on observations made with ESO Telescopes at the La Silla Paranal Observatory under programme IDs 097.C-0277(A) and 099.C-0081(A). We thank the anonymous referee for the useful comments.

REFERENCES

- Acke B., Waelkens C., 2004, *A&A*, 427, 1009
- Aldenius M., Lundberg H., Blackwell-Whitehead R., 2009, *A&A*, 502, 989

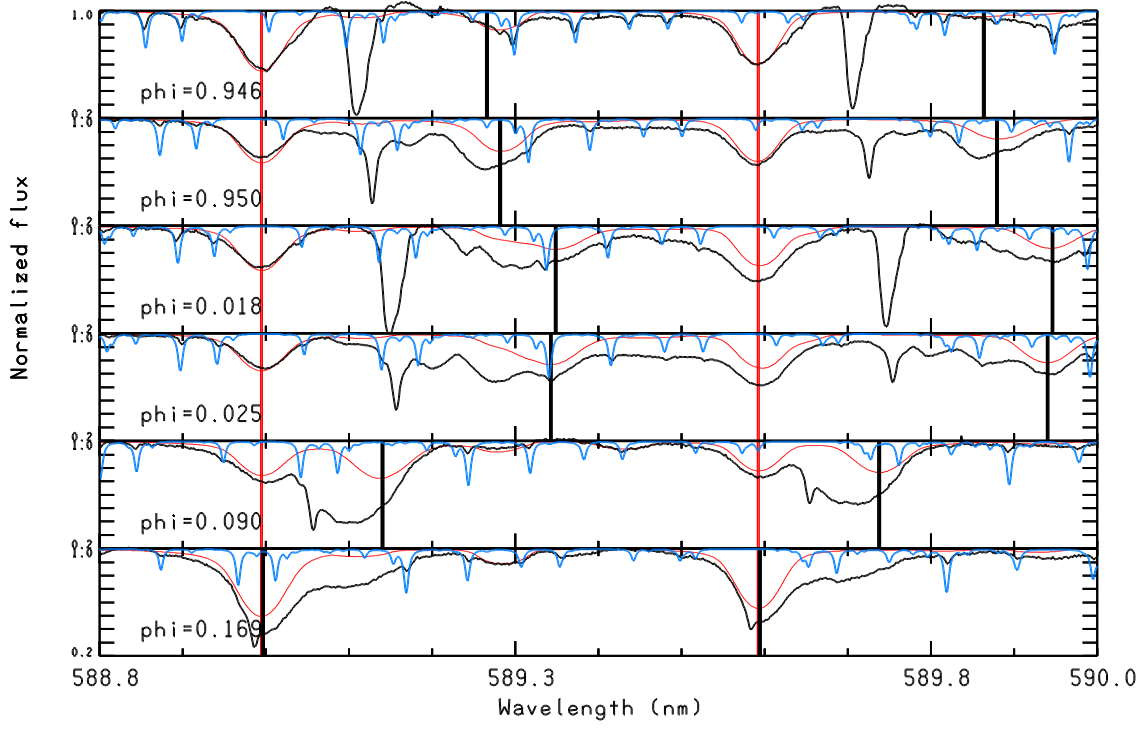


Figure 4. Comparison of the Na I doublet at 5889.95 Å and 5895.920 Å, observed at different phases, with the synthetic spectrum. The wavelength scale of the primary coincides with the laboratory wavelengths. The red and black vertical lines mark the position of the Na I lines in the primary and in the secondary, respectively. The sharp blue lines indicate contamination by telluric lines.

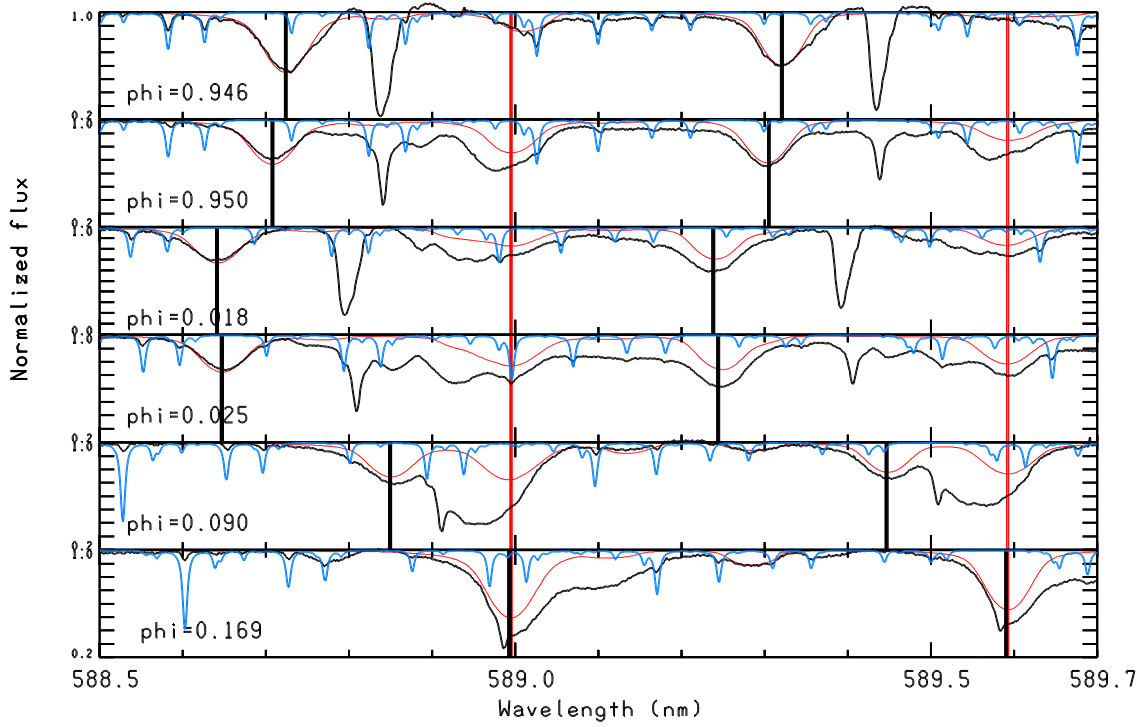


Figure 5. Comparison of the Na I doublet at 5889.95 Å and 5895.920 Å, observed at different phases, with the synthetic spectrum. The wavelength scale of the secondary coincides with the laboratory wavelengths. The red and black vertical lines mark the position of the Na I lines in the secondary and in the primary, respectively. The sharp blue lines indicate contamination by telluric lines.

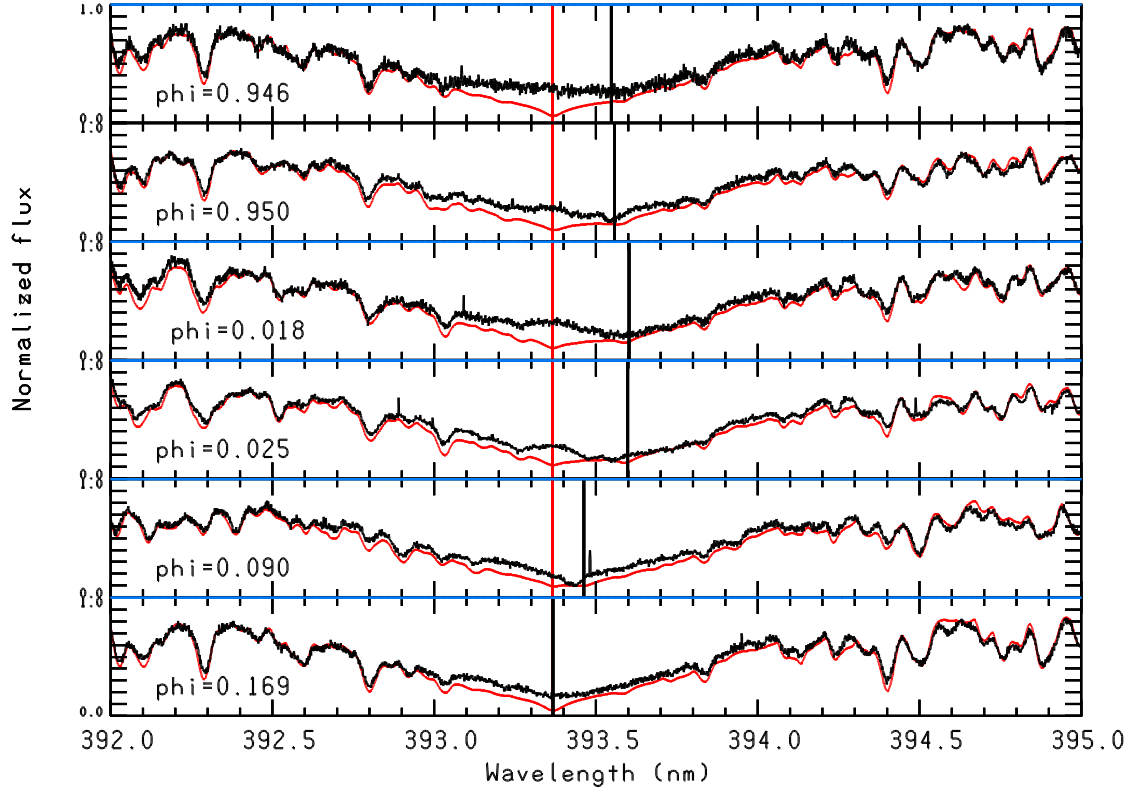


Figure 6. Comparison with the synthetic spectrum of the Ca II K line at 3933.664 \AA , observed at different phases. The wavelength scale of the primary coincides with the laboratory wavelengths. The red and black vertical lines mark the position of the Ca II K line in the primary and in the secondary, respectively.

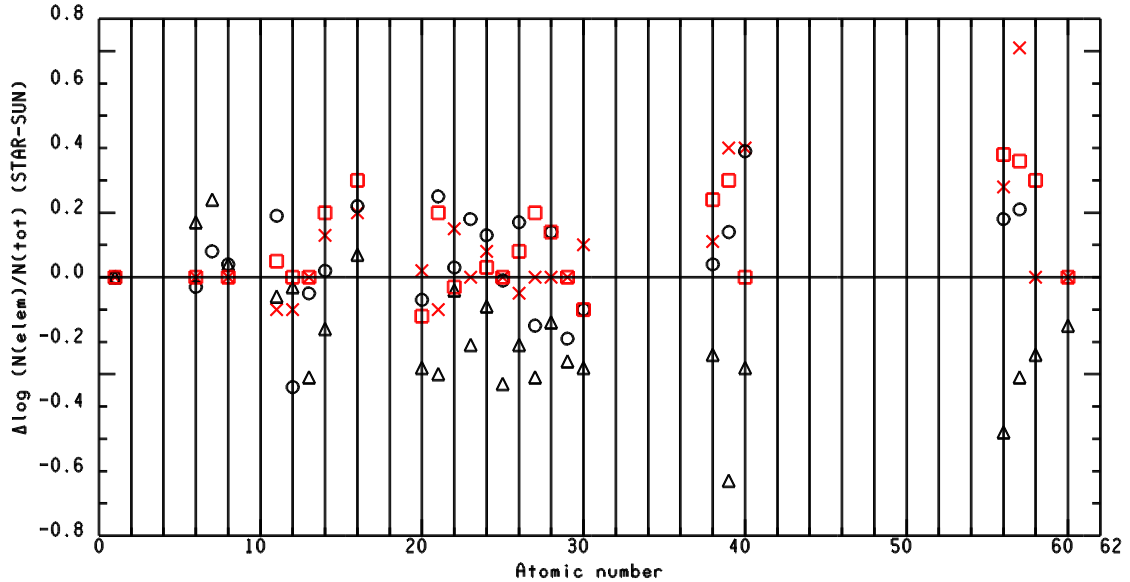


Figure 7. Comparison of the abundances relative to the solar ones of AK Sco A (red x) and AK Sco B (red boxes) with the abundances of the two magnetic Herbig Ae stars PDS2 (triangle) and HD 104237 (open circles).

Alencar S. H. P., Melo C. H. F., Dullemond C. P., Andersen J., Batalha C., Vaz L. P. R., Mathieu R. D., 2003, *A&A*, 409, 1037

Andersen J., Lindgren H., Hazen M. L., Mayor M., 1989, *A&A*, 219, 142

Anstee S. D., O'Mara B. J., 1995, *MNRAS*, 276, 859

Asplund M., Grevesse N., Sauval A. J., Scott P., 2009, *ARA&A*, 47, 481

Babcock H. W., 1958, *ApJS*, 3, 141

Barklem P. S., Piskunov N., O'Mara B. J., 2000, *VizieR Online Data Catalog*, J/A+AS/142/467

Bessell M. S., 1979, *Dudley Observatory Reports*, 14, 279

Castelli F., Kurucz R. L. 2003, in *Modelling of Stellar Atmospheres*, N. Piskunov, W. W. Weiss, & D. F. Gray, eds., *IAU Symp.*, 210, A20

Catala C., 2003, *EAS Publications Series*, 9, 325

Cowley C. R., Hubrig S., González J. F., Savanov I., 2010, *A&A*, 523, A65

Cowley C. R., Hubrig S., 2012, *Astron. Nachr.*, 333, 34

Cowley C. R., Castelli F., Hubrig S., 2013, *MNRAS*, 431, 3485

Cowley C. R., Hubrig S., Przybilla N., 2014, *MNRAS*, 440, 2457

Duchêne G., 2015, *Ap&SS*, 355, 291

Ferrario L., Pringle J. E., Tout C. A., Wickramasinghe D. T., 2009, *MNRAS*, 400, L71

Folsom C. P., Bagnulo S., Wade G. A., Alecian E., Landstreet J. D., Marsden S. C., Waite I. A., 2012, *MNRAS*, 422, 2072

Fuhr J. R., Martin G. A., Wiese W. L., 1988, *Journal of Physical and Chemical Reference Data*, 17, Suppl. 4

Garz T., 1973, *A&A*, 26, 471

Gómez de Castro A. I., 2009, *ApJ*, 698, L108

Grevesse N., Scott P., Asplund M., Sauval A. J., 2015, *A&A*, 573, A27

Herbig G. H., Kameswara Rao N., 1972, *ApJ*, 174, 401

Hubrig S., et al., 2014, *MNRAS*, 440, L6

Hubrig S., Carroll T. A., Schöller M., Ilyin I., 2015, *MNRAS*, 449, L118

Järvinen S. P., et al., 2018, *ApJ*, 858, L18

Kramida A., Ralchenko Yu., Reader J., and NIST ASD Team, 2018, *Nist Atomic Spectra Database*, [Online] available at <https://physics.nist.gov/asd/>

Kurucz R., 1993, *Atomic data for opacity calculations*. Kurucz CD-ROM No. 1. Cambridge, 1

Kurucz R. L., 1995, private communication

Kurucz R. L., 2005a, *Memorie della Societa Astronomica Italiana Supplementi*, 8, 14

Kurucz R. L., 2005b, *Memorie della Societa Astronomica Italiana Supplementi*, 8, 189

Kurucz R. L., 2018, *Astron. Soc. of the Pacific Conf. Ser.*, 515, 47

Ljung G., Nilsson H., Asplund M., Johansson S., 2006, *A&A*, 456, 1181

Michaud G., 1970, *ApJ*, 160, 641

Muzerolle J., D'Alessio P., Calvet N., Hartmann L., 2004, *ApJ*, 617, 406

Pickering J. C., Thorne A. P., Perez R., 2001, *ApJS*, 132, 403

Pogodin M. A., Hubrig S., Yudin R. V., Schöller M., González J. F., Stelzer B., 2012, *Astron. Nachr.*, 333, 594

Popper D. M., 1980, *ARA&A*, 18, 115

Raassen A. J. J., Uylings P. H. M., 1998a, *Journal of Physics B Atomic Molecular Physics*, 31, 3137

Raassen A. J. J., Uylings P. H. M., 1998b, *VizieR Online Data Catalog*, J/A+A/340/300

Reiter M., et al., 2018, *ApJ*, 852, 5

Scott P., et al., 2015a, *A&A*, 573, A25

Scott P., Asplund M., Grevesse N., Bergemann M., Sauval A. J., 2015b, *A&A*, 573, A26

Stepień K., Landstreet J. D., 2002, *A&A*, 384, 554

APPENDIX A: THE LINES ANALYZED IN THE SPECTRUM OF AK SCO

In Table A1, the lines analysed in the spectrum of AK Sco for abundance purposes are listed. Successive columns display wavelength, log gf value, the source for the log gf value, the lower excitation potential in cm^{-1} , the abundance from the primary (Star A), remarks about the given line in the primary, the abundance from the secondary (Star B), and remarks about the given line in the secondary. If the abundance was very uncertain, owing to blends or other causes, no abundance is indicated. For each examined ion the line at the top gives the average abundance for the ion under consideration and the solar abundance. If the element is present in two ionization states and different abundances from the two ions were derived, a line after the entries for the two ions gives the average abundance obtained from all lines of that element. This is the case for Si I, Si II, Ti I, Ti II, Cr I, Cr II, Fe I, Fe II, Sr I, and Sr II.

Notes to Table A1:

(^a) The index “h” added after the wavelength value indicates that hyperfine structure was considered for that line.

(^b) a “K:” at the beginning of the log gf source (Col. 3) indicates that the log gf value was taken from the Kurucz line list available at <http://kurucz.harvard.edu/linelists/gfnew/gfall08oct17.dat> and its reference from <http://kurucz.harvard.edu/linelists/gfnew/gfall.ref>; NIST5: NIST database – <http://www.nist.gov/PHYSDATA/ASD/lines-form.html> (Kramida et al. 2018); ALD: Aldenius et al. (2009); FMW: Fuhr, Martin & Wiese (1988); GARZ: Garz (1973); K88: Kurucz (1993); Ljun: Ljung et al. (2006); PTP: Pickering, Thorne & Perez (2001); RU1: Raassen & Uylings (1998a); RU2: Raassen & Uylings (1998b); SUN: astrophysical log gf value derived by fitting the observed solar profiles.

(^c) Significance of the notes in Columns 6 and 8: bl A – line blended with other lines in the primary; bl B – line blended with other lines in the secondary; bl AB – line blended with other lines in both primary and secondary; bl unk – line blended with an unidentified line; bl – line blended for other reasons; single – line unblended; almost single – line blended with a very minor component; redsh – line redshifted; core – the observed line core is weaker than the computed one; TSC – the line is computed too strong; red comp – line affected by a red component; cont – line affected by continuum.

This paper has been typeset from a $\text{\TeX}/\text{\LaTeX}$ file prepared by the author.

Table A1. Abundances for the two components of AK Sco from the ATLAS9 model with parameters $T_{\text{eff}} = 6500$ K, $\log g = 4.5$, $v_{\text{turb}} = 1.0$ and 2.0 km s^{-1} for the primary and the secondary, respectively.

λ^a [Å]	$\log gf$	Ref. ^b	χ_{low}	$\log \frac{N_Z}{N_{\text{tot(A)}}}$	Notes ^c	$\log \frac{N_Z}{N_{\text{tot(B)}}}$	Notes ^c
Li I				−8.70	−10.99 (Sun)	−8.50	−10.99 (Sun)
6707.76	−0.002	NIST5	0.000	−8.70	bl Li I	−8.50	bl Li I
6707.91	−0.303	NIST5	0.000	−8.70	bl Li I	−8.50	bl Li I
C I				−3.61	−3.61 (Sun)	−3.61	−3.61 (Sun))
4932.050	−1.658	NIST5	61981.818		bl AB		bl AB
5052.144	−1.303	NIST5	61981.818	−3.61	single		bl unk
5380.325	−1.616	NIST5	61981.818		bl B		bl A
6587.620	−1.003	NIST5	68856.338		bl AB	−3.61	single
O I				−3.35	−3.35 (Sun)	−3.35	−3.35 (Sun)
6155.961	−1.363	NIST5	86625.757	−3.35	weak, bl AB	−3.35	weak, bl AB
6155.971	−1.011	NIST5	86625.757	−3.35	weak, bl AB		weak, bl AB
6155.989	−1.120	NIST5	86625.757	−3.35	weak, bl AB		weak, bl AB
6156.737	−1.487	NIST5	86627.778	−3.35	weak, bl AB	−3.35	weak, bl AB
6156.755	−0.898	NIST5	86627.778	−3.35	weak, bl AB	−3.35	weak, bl AB
6156.778	−0.694	NIST5	86627.778	−3.35	weak, bl AB	−3.35	weak, bl AB
6158.149	−1.841	NIST5	86631.454	−3.35	weak, bl B	−3.35:	weak, bl AB
6158.172	−0.996	NIST5	86631.454	−3.35	weak, bl B	−3.35:	weak, bl AB
6158.187	−0.409	NIST5	86631.454	−3.35	weak, bl B	−3.35:	weak, bl AB
Na I				−5.93	−5.83 (Sun)	−5.78 ± 0.05	−5.83 (Sun)
4982.813h	−0.962	NIST5	16973.366		bl B		bl A
5682.633h	−0.706	NIST5	16956.172	−5.93	single	−5.73	bl
5688.193h	−1.406	NIST5	16973.368		bl B	−5.83	almost single
5688.295h	−0.452	NIST5	16973.368		bl B	−5.83	almost single
5889.950h	+0.108	NIST5	0.000		complex structure		complex structure
5895.924h	−0.194	NIST5	0.000		complex structure		complex structure
6154.225h	−1.547	NIST5	16956.170	−5.93	single		bl A
6160.747h	−1.246	NIST5	16973.366		bl B		bl A
Mg I				−4.55	−4.45 (Sun)	−4.45	−4.45 (Sun)
4057.505	−0.900	NIST5	35051.264		bl AB		bl AB
4167.271	−0.745	NIST5	35051.264	−4.55	single	−4.45	single
4702.991	−0.440	NIST5	35051.264		bl A, core TSC		bl B
5167.321	−0.870	NIST5	21850.405		bl AB, core TSC, redsh 1.5 km s^{-1}		bl AB
5172.684	−0.393	NIST5	21870.464		bl AB, core TSC, redsh 1.5 km s^{-1}		bl AB
5183.604	−0.167	NIST5	21911.178		bl A, core TSC		bl AB
5528.405	−0.498	NIST5	35051.264	−4.55	bl B, core TSC	−4.45	single
5711.095	−1.724	NIST5	35051.264		bl B	−4.46	single
Mg II				−4.55	−4.45 (Sun)	−4.45	−4.45 (Sun)
4481.126	+0.749	NIST5	71490.190	−4.55	bl B	−4.45	bl A
4481.150	−0.553	NIST5	71490.190	−4.55	bl B	−4.45	
4481.325	+0.594	NIST5	71491.063	−4.55	bl B	−4.45	
Al I				−5.61	−5.61 (Sun)	−5.61	−5.61 (Sun)
3944.006h	−0.638	NIST5	0.000	−5.61	bl B, redsh 3 km s^{-1}	−5.61	bl AB
3961.520h	−0.336	NIST5	112.061	−5.61	bl B	−5.61	bl A
6696.018h	−1.569	NIST5	25347.756		bl AB		bl AB
6698.667h	−1.870	NIST5	25347.756		single, bad cont ?		single, bad cont ?

Table A1. cont.

λ^a [Å]	$\log gf$	Ref. ^b	χ_{low}	$\log \frac{N_Z}{N_{\text{tot(A)}}}$	Notes ^c	$\log \frac{N_Z}{N_{\text{tot(B)}}}$	Notes ^c
Si I				-4.40 ± 0.07	-4.53 (Sun)	-4.31 ± 0.06	-4.53 (Sun)
5645.613	-2.140	GARZ	39760.285		bl B	-4.33	almost single
5665.555	-2.040	NIST5	39683.163		bl B		bl A
5690.425	-1.870	NIST5	39760.285	-4.33	single	-4.23	single
5708.400	-1.470	NIST5	39955.053	-4.28	almost single		bl AB
5772.146	-1.750	NIST5	40991.884	-4.28	single	-4.23	almost single
5948.541	-1.231	NIST5	40991.884	-4.43	single		bl with telluric
6091.919	-1.250	SUN	47351.554		bl AB		bl A
6125.021	-1.565	SUN	45276.188		bl AB		bl A
6142.483	-1.480	SUN	45321.848	-4.43	single	-4.33	single
6145.016	-1.411	SUN	45293.629	-4.43	single	-4.33	single
6155.134	-0.855	SUN	45321.848	-4.43	single		almost single, bad cont
6237.319	-1.070	SUN	45276.188	-4.48	single, redsh	-4.43	single
6243.815	-1.244	K:K07	45293.629	-4.48	single		bl A
6244.466	-1.291	SUN	45293.629	-4.38	single		bl A
6414.980	-1.036	K:K07	47351.554	-4.48	single		bl A
6721.848	-1.140	SUN	47284.061	-4.33	single	-4.33	single
Si II				-4.40	-4.53 (Sun)	-4.40	-4.53 (Sun)
5055.984	+0.523	NIST5	81251.320		bl AB		bl AB, telluric
6347.109	+0.149	NIST5	65500.470	-4.40	single	-4.40	single
6371.359	-0.082	NIST5	65500.470		bl B	-4.40	single
Si(tot)				-4.40 ± 0.07	-4.53 (Sun)	-4.33 ± 0.07	-4.53 (Sun)
S I				-4.72 ± 0.10	-4.92 (Sun)	-4.62 ± 0.10	-4.92 (Sun)
6046.038	-0.959	NIST5	63457.142		bl B	-4.52	single
6052.594	-1.258	NIST5	63475.051	-4.82	single		bl B
6743.552	-1.065	NIST5	63446.065		bl AB		bl A
6748.578	-0.843	NIST5	63457.142		bl unk		bl unk
6748.792	-0.638	NIST5	63457.142		bl unk		bl A, unk
6756.961	-0.937	NIST5	63477.051	-4.62	bl S I	-4.72	bl S I
6757.153	-0.351	NIST5	63475.051	-4.62	bl S I	-4.72	bl S I
Ca I				-5.70 ± 0.10	-5.72 (Sun)	-5.84 ± 0.08	-5.72 (Sun)
4226.728	+0.244	NIST5	0.000		bl AB		bl AB
4283.011	-0.224	NIST5	15210.063		bl AB		bl AB
4318.652	-0.208	NIST5	15315.943		bl A	-5.65	single
4425.437	-0.358	NIST5	15157.901	-5.72	almost single	-5.72	almost single
4434.957	-0.010	NIST5	15210.063		bl AB		bl B
4435.679	-0.519	NIST5	15210.063		bl unk ?		bl A
4578.551	-0.558	NIST5	20335.360	-5.72	single		bl unk ?
4585.865	-0.187	NIST5	20371.000		bl B		bl A
4685.268	-0.88	NIST5	44989.830	-5.57	single		bl A
5512.980	-0.300	NIST5	23652.304	-5.82	almost single		bl A
5581.965	-0.517	K:K07	20349.260	-5.57	almost single	-5.62	almost single
5590.114	-0.547	K:K07	20335.360		bl B	-5.62	almost single
5598.480	-0.091	K:K07	20335.360		bl A		bl B
5867.562	-1.600	SUN	23652.304		bl B	-5.62	single
6102.723	-0.790	NIST5	15157.901	-5.57	single	-5.62	single
6122.217	-0.315	NIST5	15210.063	-5.65	single	-5.55	single
6162.173	-0.170	ALD	15315.943	-5.65	almost single		bl AB
6169.042	-0.54	NIST5	20349.268	-5.77	almost single		bl A
6169.563	-0.27	NIST5	20371.000	-5.72	almost single		bl A
6439.075	+0.47	NIST5	20371.000	-5.70	single	-5.60	single
6449.808	-0.55	NIST5	20335.360	-5.70	almost single	-5.70	almost single
6471.662	-0.59	NIST5	20371.000	-5.70	single	-5.70	single, bl telluric
6499.650	-0.59	NIST5	20371.000	-5.95	single	-5.80	single
6717.681	-0.61	NIST5	21849.634	-5.70	almost single	-5.45	almost single, redsh 1.5 km s ⁻¹ , red comp ?

Table A1. cont.

λ^a [Å]	$\log gf$	Ref. ^b	χ_{low}	$\log \frac{N_Z}{N_{\text{tot(A)}}}$	Notes ^c	$\log \frac{N_Z}{N_{\text{tot(B)}}}$	Notes ^c
Ca II					−5.72 (Sun)		−5.72(Sun)
3933.664	0.111	K:K10	0.000		core not fitted		not fitted
3968.469	−0.194	K:K10	0.000		core not fitted		not fitted
Sc II				−8.98	−8.88 (Sun)	−8.68	−8.88 (Sun)
4246.822h	+0.242	NIST5	2540.950		bl, red comp ?		bl, red comp ?
4314.083h	−0.096	NIST5	4987.790		bl AB		bl AB
4320.732h	−0.252	NIST5	4883.570		bl A		bl AB
4400.389h	−0.536	NIST5	4883.570	−8.98	almost single		bl A
4670.407h	−0.576	NIST5	10944.560		bl AB		bl AB
5031.021	−0.399	NIST5	10944.560		bl AB	−8.68	almost single
5239.813	−0.765	NIST5	11736.360	−8.98	almost single	−8.68	almost single
5526.790h	+0.025	NIST5	14261.250		bl B, red comp ?		bl A
6604.601h	−1.309	NIST5	10944.560	−8.98	single		bl B
Ti I				−7.145 ± 0.04	−7.11 (Sun)	−7.11	−7.11 (Sun)
4286.004	−0.350	K:LGWS	6661.006	−7.11	single		bl
4512.734	−0.424	K:BMPS	6742.756	−7.21	almost single		spike
4981.731	+0.560	K:BMPS	6842.962		bl B		bl A
4999.503	+0.306	K:BMPS	6661.004		bl B		bl A
5035.903	+0.220	K:LGWS	11776.812		bl A		bl B
5039.957h	−1.074	K:BMP	170.13		bl B		no fit, bl A
5866.451h	−0.784	K:BMPS	8602.344	−7.11	single		bl A
Ti II				−6.88 ± 0.09	−7.11 (Sun)	−7.14 ± 0.09	−7.11 (Sun)
4025.129	−2.110	K:WLSC	4897.650		bl AB		bl B
4287.873h	−1.790	PTP	8710.440		bl AB		bl AB
4290.215h	−0.870	K:WLSC	9395.710		bl AB		bl AB
4300.042h	−0.460	K:WLSC	9518.060		bl AB		bl AB
4312.860h	−1.120	K:WLSC	9518.152	−6.81	single		bl A
4398.289	−2.650	K:PTP	9872.899		bl A		bl AB
4399.765h	−1.200	K:WLSC	9975.999		bl A		bl A
4411.073h	−0.650	K:WLSC	24961.030		bl A		bl B
4411.930	−2.620	K:WLSC	9872.73		bl A		bl B
4417.713h	−1.167	K:K16	9395.802		bl B		bl A
4421.938	−1.640	K:WLSC	16625.11		bl A		bl AB
4441.728	−2.333	K:K16	9518.06	−6.81	almost single		bl A
4443.801h	−0.710	K:WLSC	8710.44		red comp ?, not in syn1		bl unk ?
4450.482h	−1.520	K:WLSC	8744.25		bl AB		bl AB
4468.492h	−0.600	K:BHNG	9118.26	−6.81	single		bl A
4488.325h	−0.500	K:WLSC	25192.79		bl A		bl AB
4501.270h	−0.770	K:WLSC	8997.71		bl AB		bl AB
4518.332	−2.560	K:WLSC	8710.440		bl A		bl AB
4533.960h	−0.577	K:K16	9975.92		bl AB		bl AB
4563.758h	−0.795	K:K16	10024.73		bl AB		bl AB
4571.971h	−0.310	K:WLSC	12676.97		bl AB, red comp ?		bl B, red comp ?
4708.663	−2.350	K:WLSC	9975.92		bl B		bl A
4779.979	−1.248	K:K16	16515.86	−6.81	single	−7.01	single
4798.531	−2.660	K:WLSC	8710.44		bl A		bl AB
5010.209	−1.350	K:WLSC	25192.79		bl A		bl AB
5211.530	−1.410	K:WLSC	20891.787		bl B	−7.21	almost single
5381.022	−1.970	K:WLSC	12628.73		bl B		bl A
5418.768	−2.130	K:WLSC	12758.11	−7.01	single		bl A
5490.693	−2.663	K:K16	12628.834		bl A		bl A
6491.566	−1.942	K:K16	16625.110	−7.01:	bl telluric	−7.21	single
Ti(tot)				−6.96 ± 0.15	−7.11 (Sun)	−7.14 ± 0.09	−7.11 (Sun)

Table A1. cont.

λ^a [Å]	$\log gf$	Ref. ^b	χ_{low}	$\log \frac{N_Z}{N_{\text{tot(A)}}}$	Notes ^c	$\log \frac{N_Z}{N_{\text{tot(B)}}}$	Notes ^c
V I				−8.15	−8.15(Sun)	—	−8.15 (Sun)
4379.230h	+0.580	NIST5	2424.780	−8.15	single		bl A
6090.208h	−0.067	NIST5	8715.760	−8.15	single		bl A
6119.527h	−0.350	NIST5	8578.530		bl B		bl AB, weak
V II				—		—	−8.15 (Sun)
4002.928	−1.440	K:WLDS	11514.760		bl AB		bl AB
4023.377	−0.610	K:WLDS	14556.090		bl B		bl A
4183.428	−1.060	K:WLDS	16533.00		bl AB		bl A
4312.348	−1.495	K:BGFM	13490.883		bl AB		bl B
Cr I				−6.41 ± 0.12	−6.42 (Sun)	−6.42	−6.42 (Sun)
4254.336	−0.108	K:BMP	0.000		bl AB		bl AB
4274.797	−0.231	K:BMP	0.000		bl AB		bl AB
4616.124	−1.204	K:BMP	7927.441	−6.42	single		bl A
4626.173	−1.340	K:BMP	7810.820		bl B		bl A
4652.157	−1.035	K:SLS	8095.187		bl B	−6.42	almost single
4718.420	+0.240	K:SLS	25771.420	−6.42	almost single, redsh ?	−6.42	almost single, redsh ?
5204.511	−0.198	K:BMP	7593.160		bl A		bl AB
5208.425	+0.172	K:BMP	7593.148		bl A, flat core		bl B
5409.784	−0.715	K:BMP	8307.575	−6.22	almost single		bl AB
5787.919	−0.083	K:BBMP	26796.266	−6.57	single	−6.42	single
5790.957	+0.250	K:K16	25787.964		bl A, flat core		bl B
Cr II				−6.22 ± 0.2	−6.42 (Sun)	−6.35 ± 0.04	−6.42 (Sun)
4242.366	−1.352	K:K16	31219.350		bl AB		bl AB
4252.625	−2.053	K:K16	31117.390		bl B		bl A
4558.644	−0.444	K:K16	32854.31	−6.42	bl Cr II	−6.32	almost single
4558.788	−2.741	RU1	32854.94	−6.42	bl Cr II	−6.32	
4588.198	−0.826	K:NLLN	32836.68		bl B	−6.32	single
4616.624	−1.575	RU1	32844.76		bl AB		bl B
4618.807	−0.996	K:NLLN	32854.95		bl A		bl AB
4634.070	−0.980	K:NLLN	32844.76		bl B		bl A
4824.131	−1.085	RU1	31219.332		bl A		bl AB
5237.322	−1.160	NIST5	32854.31		bl AB	−6.42	almost single
5502.085	−2.048	K:K16	33618.91	−6.02	single		bl A
Cr(tot)				−6.34 ± 0.17	−6.42 (Sun)	−6.39 ± 0.02	−5.42 (Sun)
Mn I				−6.62	−6.62 (Sun)	−6.62	−6.62 (Sun)
4033.062h	−0.647	K:DLSS	0.000		bl AB		bl B
4034.483h	−0.843	K:DLSS	0.000	−6.62	single		bl A
4041.355h	+0.281	K:DLSS	17052.29		bl A		bl B
4754.042h	−0.080	K:DLSS	23719.52	−6.62	almost single	−6.62	almost single
4783.427h	+0.044	K:DLSS	18531.5	−6.62	almost single	−6.62	single
4823.524h	+0.136	K:DLSS	18705.2		bl A		bl B
5377.596h	−0.166	K:K07	31001.153		bl B		bl A
5537.765h	−2.017	K88	17637.156		bl AB		bl AB
6013.510h	−0.354	K:DLSS	24779.331		red comp ?, only $\phi = 0.090$		red comp ?, only $\phi = 0.090$

Table A1. cont.

λ^a [Å]	$\log gf$	Ref. ^b	χ_{low}	$\log \frac{N_Z}{N_{\text{tot(A)}}}$	Notes ^c	$\log \frac{N_Z}{N_{\text{tot(B)}}}$	Notes ^c
Fe I				-4.66 ± 0.15	-4.57 (Sun)	-4.51 ± 0.17	-4.57 (Sun)
4071.738	-0.022	K:FW	12968.554		bl AB		bl AB
4383.544	+0.200	K:FW	11976.239		bl A		bl AB
4736.773	-0.67	K:DRLP	25899.899		bl B	-4.57	single
4890.755	-0.38	K:RDLB	23192.500		bl A		bl B
4891.492	-0.112	K:FW	22996.674	-4.67	single		bl A
4903.310	-0.89	K:RDLB	23244.838		bl A		bl AB
4907.732	-1.70	K:DRLP	27666.348		bl A		bl AB
4909.383	-1.325	K:K17	31686.351		bl B		bl A
4917.230	-1.66	K:FW	33801.572	-4.57	single		bl A
4918.954	-0.602	K:K17	33507.123	-4.57	bl Fe I		bl AB
4918.994	-0.342	K:FW	23110.939	-4.57	bl Fe I	-4.57	bl AB
4920.502	+0.07	K:RDLB	22845.869		bl AB, core		very bl AB
4946.387	-1.11	K:RDLB	27166.820		bl AB		bl A
4950.105	-1.50	K:DRLP	27559.583		single, bad cont ?	-4.37	single
4957.596	+0.233	K:FW	22650.416		bl A, core		bl AB
4962.571	-1.182	K:FW	33695.397		bl B	-4.27	single
4969.917	-0.588	K:K17	34017.103		bl B		bl A
4970.496	-1.74	K:FW	29320.025		bl A		bl B
4991.268	-0.368	K:K17	33801.572		bl AB, core		bl B
4994.129	-3.080	K:FW	7376.764		bl B		bl B
5007.274	-0.198	K:K17	33095.941		bl AB, core		bl AB
5028.126	-1.02	K:RDLB	28819.954		bl B		bl A
5068.766	-1.042	K:FW	23711.456		bl AB		bl B
5098.698	-2.03	K:FW	17550.181		bl AB, red comp ?		bl AB
5107.447	-3.087	K:FW	7985.785		bl A		bl B
5107.641	-2.418	K:FW	12560.934	-4.57	bl A	-4.27	bl B
5110.413	-3.760	K:FW	0.000		bl A, core		bl B
5126.192	-1.06	K:FW	34328.752		bl B, unk, redsh ?		bl A, unk ?
5137.381	-0.43	K:FW	33695.397		bl AB, redsh		bl B
5142.494	-0.739	K:K17	34692.148		bl AB, redsh		bl AB, core
5142.540	-0.295	K:K17	34328.752	-4.57	bl AB, redsh	-4.27	bl AB, core
5196.059	-0.477	K:K17	34328.752		bl AB, redsh ?		bl AB
5216.274	-2.150	K:FW	12968.554		bl AB, red comp ?		bl AB
5217.389	-1.07	K:DRLP	25899.989		bl AB, redsh ?	-4.57	single
5232.940	-0.057	K:FW	23711.456	-4.67	almost single		bl A
5364.870	+0.228	K:FW	35856.402	-4.67	single	-4.57	single
5367.465	+0.443	K:FW	35611.625	-4.97	almost single, core	-4.87	almost single, core
5369.961	+0.536	K:FW	35257.324	-4.77	almost single		bl A
5371.489	-1.645	K:FW	7728.060		bl AB		bl AB
5373.708	-0.71	K:RDLB	36079.372		bl AB		bl B
5383.368	+0.645	K:FW	34782.421		bl B	-4.57	almost single
5389.478	-0.430	K:K17	35611.625	-4.67	almost single	-4.47	almost single
5400.501	-0.151	K:K17	35257.324		bl AB		bl AB
5405.774	-1.844	K:FW	7985.785		bl AB		bl A
5410.909	+0.398	K:FW	36079.372		bl AB, redsh, red comp ?	-4.47	almost single
5415.198	+0.642	K:FW	35279.308		bl AB	-4.67	almost single
5424.067	+0.780	K:K17	34843.957		bl A, core		bl AB, core
5429.696	-1.879	K:FW	7728.060		bl A		bl AB
5445.042	+0.209	K:K17	35379.208	-4.82	single, core		bl AB
5446.916	-1.914	K:FW	7985.785		bl AB		bl AB
5466.395	-0.630	FMW	35257.324		bl A		bl A
5487.745	-0.316	K:K17	34843.957	-4.67	single, core		bl AB
5497.516	-2.849	K:FW	8154.714		bl A		bl B, core
5506.779	-2.797	K:FW	7985.785		bl A		bl B
5522.446	-1.52	K:FW	33946.933		bl B		bl A
5560.212	-1.16	K:FW	35767.564	-4.47	single, core		bl A
5572.842	-0.28	K:DRLP	27394.691		bl A, core		bl AB
5914.111	-0.362	K:K17	37162.764		bl A, core		bl B
5914.201	-0.111	K:K17	37162.764	-4.47	bl A, core	-4.67	bl B
6191.557	-1.416	K:FW	19621.006		bl A		bl B
6393.600	-1.58	K:FW	19621.006	-4.37	single, redsh 1 km s^{-1} ?, comp ?	-4.27	single

Table A1. cont.

λ^a [Å]	$\log gf$	Ref. ^b	χ_{low}	$\log \frac{N_z}{N_{\text{tot(A)}}}$	Notes ^c	$\log \frac{N_z}{N_{\text{tot(B)}}}$	Notes ^c
Fe II				−4.42	−4.37 (Sun)	−4.44 ± 0.06	−4.57 (Sun)
4178.854	−2.535	RU2	20830.582		bl B, unk		bl A
4413.591	−3.985	SUN	21581.638	−4.42	single		very bl
4416.819	−2.601	RU2	22409.852		bl B		bl A
4515.533	−2.540	RU2	22409.852		bl AB, redsh		bl AB
4620.513	−3.188	K:FW	22810.357		bl B		bl A, redsh ?
4635.317	−1.474	K:FW	48039.090		bl B		bl A
4923.921	−1.206	K:FW	23317.635		bl AB		bl AB
5100.655	−4.222	K:FW	22637.195		bl B	−4.32	bl Fe II
5120.344	−4.275	K:K13	22810.357		bl AB		bl AB
5132.661	−4.008	K:FW	22637.205		bl B		bl A
5197.568	−2.229	K:FW	26055.412		bl A, red wing, unk ?		bl A
5362.869	−2.616	RU2	25805.327		bl AB		bl AB
5425.249	−3.352	K:FW	25805.327		bl B	−4.47	single
5534.838	−2.86	K:FW	26170.18	−4.42	single	−4.47	single
6084.102	−3.854	K:FW	25805.327		bl B		bl unk ?
6147.734	−2.731	K:FW	31364.455		bl A, Fe I		bl AB
6149.246	−2.732	K:FW	31368.453		bl B	−4.47	single
6383.730	−2.275	K:FW	60445.279		bl A, Fe I		bl AB
6456.380	−2.086	K:FW	31483.198		bl B	−4.47	single
Fe(tot)				−4.62 ± 0.16	−4.57 (Sun)	−4.49 ± 0.15	−4.57 (Sun)
Co I				—	−7.11 (Sun)	−6.91	−7.11 (Sun)
3995.302h	−0.220	NIST5	7442.410		bl AB	−6.91	single
4118.767h	−1.093	K:K08	8460.783		bl AB		bl A
4121.311h	−0.320	NIST5	7442.410		bl B		bl A
Ni I				−5.84 ± 0.08	−5.84 (Sun)	−5.70 ± 0.17	−5.84 (Sun)
4295.882h	−0.480	NIST5	30979.749		bl AB		bl AB
4648.652	−0.150	NIST5	27580.391		bl B		bl A
4701.530	−0.390	NIST5	32973.376		bl AB		bl AB
4756.515	−0.270	NIST5	28068.065	−5.84	almost single		bl A
4806.987	−0.640	NIST5	29668.893	−5.84	single		bl A
4829.023h	−0.330	NIST5	28569.203	−5.84	almost single	−5.84	almost single
4831.176	−0.410	NIST5	29084.450	−5.94	single		bl A
4904.412h	−0.170	NIST5	28569.203		bl B	−5.84	single
5035.362h	+0.290	NIST5	29320.762	−5.94	single	−5.84	single
5035.967h	−0.234	K88	29480.989		bl A		bl B
5081.110	+0.300	NIST5	31031.020		bl B		bl A
5082.344h	−0.540	NIST5	29500.674		bl B		bl A
5085.480h	−1.480	NIST5	29500.674		bl B	−5.84	single
5099.920	−0.100	NIST5	29668.893		bl B	−5.74	single
5102.960h	−2.620	NIST5	13521.347	−5.94	single		bl A
5115.392	−0.110	NIST5	30922.734		bl B		bl A
5146.482h	+0.060	K:K08	29888.477		bl A		bl B
5155.764	−0.090	NIST5	31441.635		bl B	−5.44	single
5578.726	−2.640	NIST5	13521.347	−5.74	single	−5.44	single, spike, cont
6643.543h	−2.300	NIST5	13521.347	−5.74	single	−5.59	single
6772.315	−0.990	NIST5	29500.674	−5.74	single		bl A
Cu I				−7.86	−7.86 (Sun)	−7.86	−7.86 (Sun)
5105.548	−1.500	NIST5	11202.565	−7.86:	bl B	−7.86	single
5153.238	+0.116	K:K12	30535.302		bl B		bl A
5218.202	+0.264	NIST5	30783.686		bl A		bl A

Table A1. cont.

λ^a [Å]	$\log gf$	Ref. ^b	χ_{low}	$\log \frac{N_Z}{N_{\text{tot(A)}}}$	Notes ^c	$\log \frac{N_Z}{N_{\text{tot(B)}}}$	Notes ^c
Zn I				−7.38:	−7.48 (Sun)	−7.58	−7.48 (Sun)
4680.136	−0.810	K:K12	32311.319		bl AB		bl AB
4722.157	−0.338	K:K12	32501.330		bl B		bl A
4810.532	−0.125	K:K12	32890.327	−8.08?	single, bad cont ?	−8.08 ?	single, bad cont ?
6362.346	+0.160	NIST5	46771.199	−7.38:	bl B	−7.58	single
Sr I				—	−9.21 (Sun)	−9.0	−9.21 (Sun)
4607.333	+0.283	NIST5	0.000		bl B	−9.00	single
Sr II				−9.10	−9.21 (Sun)	−8.90	−9.21 (Sun)
4077.709	+0.148	NIST5	0.000		bl AB		bl AB
4215.519	−0.173	NIST5	0.000	−9.1	bl A	−8.9	bl AB
4305.443	−0.11	NIST5	24516.65		bl AB		bl B
Sr(tot)				−9.1	−9.21 (Sun)	−8.95 ± 0.05	−9.21 (Sun)
Y II				−9.40	−9.83 (Sun)	−9.50	−9.83 (Sun)
4177.530h	−0.163	NIST5	3296.180		bl AB		bl B
4309.622	−0.747	NIST5	1449.752		bl A		bl B
4374.933h	+0.155	NIST5	3296.184		bl AB		bl AB
4398.010	−0.999	NIST5	1045.083		bl A		bl A
4854.861h	−0.38	NIST5	8003.126		bl B		bl B
4883.682h	+0.07	NIST5	8743.316	−9.40	single		bl A, cont ?
4900.119h	−0.09	NIST5	8328.041		cont ?, bl A		cont ?, bl B
5087.419h	−0.17	NIST5	8743.316	−9.40	single	−9.50	bl A
5119.112h	−1.36	NIST5	8003.121		bl A		bl AB
5205.723h	−0.35	NIST5	8328.039		bl AB		bl B
5509.895h	−1.015	NIST5	8003.126		bl A		bl B
Zr II				−9.04	−9.45 (Sun)	−9.45	−9.45 (Sun)
4149.198	−0.040	Ljun	6467.610		bl A		bl AB
4156.232	−0.780	Ljun	5724.380		bl unk		bl unk
4208.980	−0.510	Ljun	5752.920	−9.04	single	−9.45	single
4258.041	−1.200	Ljun	4505.500		bl A		bl AB
4442.992	−0.420	Ljun	11984.460		bl AB		bl AB
4496.962	−0.890	Ljun	5752.92		bl A		bl AB
5112.270	−0.850	Ljun	13428.500	−9.04	single		bl A
Ba I					−9.79 (Sun)		−9.79 (Sun)
5535.481	+0.215	NIST5	0.000		bl A		bl AB
Ba II				−9.51	−9.79 (Sun)	−9.41	−9.79 (Sun)
4130.649	+0.524	NIST5	21952.36		bl A		bl A
4554.033h	+0.140	NIST5	0.000	−9.51	almost single	−9.41	almost single
4934.077h	−0.157	NIST5	0.000		bl AB		bl A
5853.675	−0.908	NIST5	4873.852		bl B		bl A
6141.710	−0.032	NIST5	5674.807		bl A		bl B
6496.898h	−0.407	NIST5	4873.852		bl telluric		bl telluric

Table A1. cont.

λ^a [Å]	$\log gf$	Ref. ^b	χ_{low}	$\log \frac{N_Z}{N_{\text{tot(A)}}}$	Notes ^c	$\log \frac{N_Z}{N_{\text{tot(B)}}}$	Notes ^c
La II				-10.22 ± 0.15	-10.93 (Sun)	-10.57	-10.93 (Sun)
3988.515h	+0.210	NIST5	3250.35		bl A		bl A
3995.745	-0.064	NIST5	1394.46		cont		bl AB
4042.901	+0.270	L:CB'	7473.32	-10.37	single		bl A
4086.709h	-0.070	NIST5	0.000		bl B	-10.57	single
4123.218h	+0.130	NIST5	2591.60		bl AB		bl B
4333.75	-0.059	NIST5	1394.46	-10.07	single		bl A
Ce II				-10.46	-10.46 (Sun)	—	-10.46 (Sun)
4186.596	0.813	K:MC	6967.547		bl A		bl B
4562.358	0.210	NIST5	3854.012		bl B		bl A
4628.161	0.140	NIST5	4165.55	-10.46	single		bl A
Nd II				$-10.62 ?$	-10.62 (Sun)	$-10.62 ?$	-10.62 (Sun)
4061.080	+0.550	NIST5	3801.93	-10.62	bl A	-10.62	bl B
4109.071	-0.163	NIST5	513.330	-9.98	bl AB	-9.98	bl AB
4303.571	+0.084	NIST5	0.000	-10.62	bl B	-10.62	bl A
4706.543	-0.710	NIST5	0.000	-9.92	bl B	-9.92	single
5076.580	-0.250	K:MC'	5985.59	> -10.62	bl A	-10.62	bl B